The 8th European Congress on Computational Methods in Applied Sciences and Engineering
ECCOMAS Congress 2022
5-–9 June 2022, Oslo, Norway

USING A REDUCED SET OF FOURIER MODES IN TERMS OF A FFT-BASED MICROSTRUCTURE SIMULATION

CHRISTIAN GIERDEN[1], JOHANNA WAIMANN[1], BOB SVENDSEN[2,3] AND STEFANIE REESE[1]

[1] Institute of Applied Mechanics
RWTH Aachen University
Mies-van-der-Rohe-Straße 1, D-52074 Aachen, Germany
e-mail: {christian.gierden, johanna.waimann, stefanie.reese}@rwth-aachen.de,
www.ifam.rwth-aachen.de

[2] Material Mechanics
RWTH Aachen University
Schinkelstraße 2, D-52062 Aachen, Germany
www.cmm.rwth-aachen.de

[3] Microstructure Physics and Alloy Design
Max-Planck-Institut für Eisenforschung GmbH
Max-Planck-Straße 1, D-40237 Düsseldorf, Germany
e-mail: b.svendsen@mpie.de
www.mpie.de

Key words: Microstructure simulation, FFT, Spectral solver, Model order reduction

Abstract. Given a heterogeneous material, the mechanical behavior of its microstructure can be investigated by an algorithm that uses the Fourier representation of the Lippmann-Schwinger equation. Incorporating a model order reduction technique based on calculations with a reduced set of Fourier modes, the computational cost of this algorithm can be decreased. It was shown that the accuracy of this model order reduction technique strongly depends on the choice of Fourier modes by considering a geometrically adapted rather than a fixed sampling pattern to define the reduced set of Fourier modes. Since it is difficult to define a geometrically adapted sampling pattern for complex microstructures, additionally a strain-based sampling pattern was introduced. The accuracy and adaptability of this strain-based reduced set of Fourier modes is shown by incorporating a polycrystalline microstructure.

1 INTRODUCTION

Constitutive equations are usually based on a number of assumptions and even with a large number of material parameters, it is not always possible to fit the developed model to the actual material behavior. In contrast to that, multi-scale methods allow the consideration of physical and topological details of an evolving microstructure and thus an accurate representation of the resulting material behavior. In this context, a method using the finite element (FE) method on the macroscale and the fast Fourier transform (FFT) method on the microscale was introduced

in [23] for the simulation of two-phase microstructures, while the FFT-based microstructure simulation was established by Moulinec and Suquet [17, 18]. An extension of the FFT-based microstructure simulation and FE-FFT-based two-scale simulation concerning polycrystalline materials was presented in [14, 15] and [9]. General reviews presenting the state of the art of the FFT-based and FE-FFT-based methods are given in [22, 16] and [7], respectively.
A drawback of such a highly resolved two-scale simulation is the extensive computational effort. Therefore, efficient two-scale solution strategies have been introduced using for example a coarse discretized microstructure for the entire simulation considering small [10] or finite [4] strains, or using a precomputed database in general and the highly resolved microstructure simulation only in macroscopic critical areas [12]. Other model order reduction (MOR) techniques are aiming exclusively at an efficient FFT-based microstructure simulation taking into account a proper orthogonal decomposition (POD) [2], low-rank tensor approximations [25] or a reduced set of Fourier modes [11].
The focus of the present paper lies on the FFT-based microstructure simulation based on a reduced set of Fourier modes. This MOR technique was first introduced considering a fixed sampling pattern [11]. Since the accuracy of the method strongly depends on the choice of considered Fourier modes, an improvement in accuracy was achieved by using a geometrically adapted [5] or a strain-based [6] sampling pattern. In this work, we show how such a strain-based sampling pattern for the reduced FFT-based microstructure simulation is also suitable to capture the details of a complex microstructure, such as a polycrystal.
The paper is structured as follows: In Section 2 a brief review of the microstructural relations considering a polycrystalline microstructure is given. After presenting the approach for the reduced FFT-based microstructure simulation considering a strain-based sampling pattern in Section 3, the numerical results are discussed in Section 4. The paper ends with a conclusion and outlook in Section 5.

2 MICROSTRUCTURAL BOUNDARY VALUE PROBLEM

The quasi-static balance of linear momentum in absence of body forces on the microscale and taking into account small strain kinematics for a heterogeneous microstructure Ω yields

$$\operatorname{div} \boldsymbol{\sigma}(\bar{\boldsymbol{x}}, \boldsymbol{x}) = \mathbf{0} \quad \forall \boldsymbol{x} \in \Omega \,, \tag{1}$$

with the stress $\boldsymbol{\sigma}(\bar{\boldsymbol{x}}, \boldsymbol{x}) = \boldsymbol{\sigma}(\bar{\boldsymbol{x}}, \boldsymbol{x}, \boldsymbol{\varepsilon}(\bar{\boldsymbol{x}}, \boldsymbol{x}), \boldsymbol{\gamma}(\boldsymbol{x}))$ depending on the macroscopic and microscopic positions $\bar{\boldsymbol{x}}$ and $\boldsymbol{x}$, the total strain field $\boldsymbol{\varepsilon}(\bar{\boldsymbol{x}}, \boldsymbol{x})$ and internal variables $\boldsymbol{\gamma}(\boldsymbol{x})$. The total strain field $\boldsymbol{\varepsilon}(\bar{\boldsymbol{x}}, \boldsymbol{x}) = \bar{\boldsymbol{\varepsilon}}(\bar{\boldsymbol{x}}) + \tilde{\boldsymbol{\varepsilon}}(\bar{\boldsymbol{x}}, \boldsymbol{x})$ may additively be split into a constant macroscopic part $\bar{\boldsymbol{\varepsilon}}(\bar{\boldsymbol{x}})$ and a microscopic fluctuating part $\tilde{\boldsymbol{\varepsilon}}(\bar{\boldsymbol{x}}, \boldsymbol{x})$, while the macroscopic stress $\bar{\boldsymbol{\sigma}}(\bar{\boldsymbol{x}})$ and strain $\bar{\boldsymbol{\varepsilon}}(\bar{\boldsymbol{x}})$ are defined via the volume averages of their local fields:

$$\bar{\boldsymbol{\sigma}}(\bar{\boldsymbol{x}}) := \frac{1}{V} \int_{\Omega} \boldsymbol{\sigma}(\bar{\boldsymbol{x}}, \boldsymbol{x}) \, \mathrm{d}\Omega \quad \text{and} \quad \bar{\boldsymbol{\varepsilon}}(\bar{\boldsymbol{x}}) := \frac{1}{V} \int_{\Omega} \boldsymbol{\varepsilon}(\bar{\boldsymbol{x}}, \boldsymbol{x}) \, \mathrm{d}\Omega \,. \tag{2}$$

Regarding the constitutive relations, a polycrystalline microstructure is taken into account. For the sake of clarity, the dependence of all variables on the macroscopic and microscopic positions $\bar{\boldsymbol{x}}$ and $\boldsymbol{x}$ are not shown in what follows. A general overview of constitutive laws and kinematics for crystal plasticity is given in [20]. Focusing on elasto-viscoplastic polycrystalline microstructures

at small strains, the elastic stress-strain relation is defined by the linear relation $\boldsymbol{\sigma} = \mathbb{C} : \boldsymbol{\varepsilon}_e$ with an additively split of the total strain $\boldsymbol{\varepsilon} = \boldsymbol{\varepsilon}_e + \boldsymbol{\varepsilon}_p$ into an elastic part $\boldsymbol{\varepsilon}_e$ and a plastic part $\boldsymbol{\varepsilon}_p$ at each microscopic position $\boldsymbol{x} \in \Omega$. Considering only the dislocation slip as a plastic deformation process, it is assumed that the evolution of the plastic strain is the sum of the contributions of the individual slip systems α:

$$\dot{\boldsymbol{\varepsilon}}_p = \sum_{\alpha=1}^{n_{slip}} \dot{\gamma}_\alpha \, \boldsymbol{m}_\alpha^s \,. \tag{3}$$

Here, $\dot{\gamma}_\alpha$ represents the plastic shear rate and $\boldsymbol{m}_\alpha^s = \frac{1}{2}(\boldsymbol{d}_\alpha \otimes \boldsymbol{n}_\alpha + \boldsymbol{n}_\alpha \otimes \boldsymbol{d}_\alpha)$ denotes the symmetric Schmid tensor with the slip direction $\boldsymbol{d}_\alpha$ and the slip plane normal $\boldsymbol{n}_\alpha$. The plastic shear rate is assumed to follow a Perzyna-type flow rule [19]

$$\dot{\gamma}_\alpha = \dot{\gamma}_0 \, \mathrm{sgn}(\tau_\alpha) \left\langle \frac{|\tau_\alpha| - \tau^c}{\tau^d} \right\rangle^p \,, \tag{4}$$

while $\tau_\alpha = \boldsymbol{\sigma} \cdot \boldsymbol{m}_\alpha^s$ is the resolved shear stress within slip system α, τ^c is the critical resolved shear stress and $\dot{\gamma}_0$, τ^d and p are the reference shear rate, drag stress and rate sensitivity parameter. The critical resolved shear stress $\tau^c = \tau^c(\gamma_{\mathrm{acc}})$ is depending on the accumulated plastic slip $\gamma_{\mathrm{acc}} = \sum_\alpha \int |\dot{\gamma}_\alpha| \, \mathrm{d}t$ and it is assumed to follow the Voce-type isotropic hardening behavior

$$\tau^c(\gamma_{\mathrm{acc}}) = \tau_0^c + (\tau_\infty - \tau_0^c) \tanh\left(\frac{(h_0 - h_\infty)\gamma_{\mathrm{acc}}}{\tau_\infty - \tau_0^c} \right) + h_\infty \, \gamma_{\mathrm{acc}} \,, \tag{5}$$

with τ_0^c, τ_∞, h_0 and h_∞ as the initial critical resolved shear stress, the saturation shear stress, the initial hardening modulus and the saturation hardening modulus, respectively.
Regarding the numerical implementation, the flow rule (Equation (4)) is discretized using an implicit Euler scheme, while we use the enhanced power law subroutine introduced in [29]. The unknown stress $\boldsymbol{\sigma}$ and critical resolved shear stress τ_c are obtained by solving the local set of equilibrium equations

$$\begin{pmatrix} \boldsymbol{r}_{\boldsymbol{\sigma}} \\ r_\tau \end{pmatrix} = \begin{pmatrix} \boldsymbol{\varepsilon}_e^{i+1} - \mathbb{C}^{-1} : \boldsymbol{\sigma}^i \\ \tau_c^{i+1} - \tau_c^i \end{pmatrix} \stackrel{!}{=} \begin{pmatrix} \boldsymbol{0} \\ 0 \end{pmatrix} \tag{6}$$

with i being the iteration number.

3 REDUCED FFT-BASED MICROSTRUCTURE SIMULATION

To solve the microscopic balance of linear momentum (Equation (1)) for periodic microstructures, the FFT-based simulation approach [17, 18] may be used. Therefore, the polarization stress $\boldsymbol{\tau} = \boldsymbol{\sigma}(\boldsymbol{\varepsilon}) - \mathbb{C}^0 : \boldsymbol{\varepsilon}$, defined as the difference of the present stress and the stress within an isotropic homogeneous reference material behavior $\mathbb{C}^0$, is introduced [8]. This leads to a reformulation of the balance of linear momentum as

$$\mathrm{div}\left[\boldsymbol{\tau} + \mathbb{C}^0 : \boldsymbol{\varepsilon}\right] = \boldsymbol{0} \quad \forall \boldsymbol{x} \in \Omega \,, \tag{7}$$

which may be solved using the Lippmann-Schwinger equation [13]:

$$\boldsymbol{\varepsilon} = \bar{\boldsymbol{\varepsilon}} - \Gamma^0 * \boldsymbol{\tau} \quad \forall \boldsymbol{x} \in \Omega \tag{8}$$

Here, $*$ represents the convolution integral between the Lippmann-Schwinger operator Γ^0 and the polarization stress τ. To solve this equation, it is transferred into Fourier space

$$\hat{\varepsilon}(\boldsymbol{\xi}) = \begin{cases} -\hat{\Gamma}^0(\boldsymbol{\xi}) : \hat{\boldsymbol{\tau}}(\boldsymbol{\xi}) & \text{for } \boldsymbol{\xi} \neq \mathbf{0} \\ \bar{\boldsymbol{\varepsilon}} & \text{for } \boldsymbol{\xi} = \mathbf{0} \end{cases} \tag{9}$$

with $\hat{(\cdot)}$ referring to any quantity in Fourier space and $\boldsymbol{\xi}$ representing the wave vector, which gathers all the considered Fourier modes. The Lippmann-Schwinger operator in Fourier space is explicitly known as

$$\hat{\Gamma}^0(\boldsymbol{\xi}) = \frac{1}{2}\left(\hat{G}^0_{ik}\,\xi_j + \hat{G}^0_{jk}\,\xi_i\right)\xi_l \quad \text{with} \quad (\hat{G}^0_{jm})^{-1} = \mathbb{C}^0_{jkmn}\,\xi_k\,\xi_n \quad \text{for } \boldsymbol{\xi} \neq \mathbf{0}\,. \tag{10}$$

Moulinec and Suquet [17, 18] introduced a solution procedure, which makes use of this Fourier representation of the Lippmann-Schwinger equation and a fixed point solver. In order to decrease the computational effort of this simulation approach a MOR technique was introduced in [11] which reduces the computations in Fourier space by taking into account only a reduced set of Fourier modes. The accuracy of this technique directly depends on the number, but also on the choice of incorporated Fourier modes. Therefore, in [5] a choice of modes based on the representation of phases within a two-phase microstructure was introduced. This leads to an increase in accuracy, especially in the linear elastic case. To further improve the accuracy of the method for nonlinear material behavior a strain-based choice of Fourier modes was introduced in [6]. Therefore, the considered sampling pattern is updated after each load step by taking into account the norm of the strain field of the current load step and transferring it into Fourier space to define the sampling pattern $\mathcal{S}_\varepsilon$ for the next load step:

$$\mathcal{S}_\varepsilon^{i+1}: \text{ Use Fourier modes with highest amplitudes of } \hat{\varepsilon}^i_{L^2}(\boldsymbol{\xi}) = \mathrm{FFT}\{||\boldsymbol{\varepsilon}^i(\boldsymbol{x})||\} \tag{11}$$

Such a strain-based sampling pattern also leads to accurate results when considering complex microstructures, such as polycrystals, which will be shown in the following section.

4 NUMERICAL RESULTS

Let us consider a polycrystalline microstructure with 100 grains and the material parameters of copper for a reference shear rate of $\dot{\gamma}_0 = 10^{-3}\,1/s$ (cf. [15]) as shown in Figure 1, while the 12 slip systems of face-centered cubic (fcc) crystals are given by $\boldsymbol{d}_\alpha\{111\}$ and $\boldsymbol{n}_\alpha = [110]$.

Since we just considered the microscale simulation, we prescribed any macroscopic load, i.e. $\bar{\varepsilon}_{11} = 0.01$ and $\bar{\varepsilon}_{22} = -0.01$, but also any other macroscopic strain would be reasonable. The investigated microstructure is discretized by $n = 255 \times 255$ equidistant grid points and the results of the reduced FFT-based simulation are evaluated by considering the following microscopic and macroscopic error measurements:

$$\bar{\mathcal{E}} = \frac{||\bar{\boldsymbol{\sigma}} - \bar{\boldsymbol{\sigma}}^{\mathrm{ref}}||}{||\bar{\boldsymbol{\sigma}}^{\mathrm{ref}}||} \quad \text{and} \quad \mathcal{E} = \frac{1}{n}\sum_n \frac{||\boldsymbol{\sigma}(n) - \boldsymbol{\sigma}^{\mathrm{ref}}(n)||}{||\boldsymbol{\sigma}^{\mathrm{ref}}(n)||} \tag{12}$$

Here, $(\cdot)_{\mathrm{ref}}$ refers to any quantity of the reference solution in which the full set of Fourier modes was utilized. In addition, the microstructural stress difference $\Delta\sigma_{11} = |\sigma_{11} - \sigma^{\mathrm{ref}}_{11}|$, exemplarily

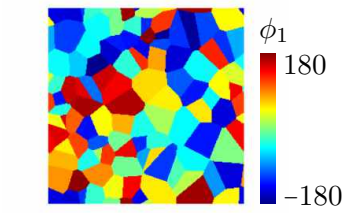

Material parameters
$C_{11} = 170.2$ GPa, $C_{12} = 114.9$ GPa, $C_{44} = 61.0$ GPa
$\tau_d = 10$ MPa, $p = 20$
$\tau_0^c = 0.1$ MPa, $\tau_\infty = 31$ MPa, $h_0 = 51$ MPa, $h_\infty = 1$ MPa

Figure 1: Microstructure with the orientation of the first Eulerian angle ϕ_1.

for the 11-component, is investigated.
Figure 2 shows the evolution of the norm of the strain field $||\boldsymbol{\varepsilon}||$ and the identified strain-based sampling pattern for $\mathcal{R} \approx 0.8\,\%$ of considered Fourier modes for load steps 2, 20, 50 and 100 (from left to right). In the first load step, the full set of Fourier modes is used. In the beginning, the material behaves elastically until the critical resolved shear stress is exceeded. Therefore, the differences within the strain field and thus within the strain-based sampling pattern are most significant within the first load steps (cf. step 2 and 20). After that, only small differences occur.
The resulting stress fields σ_{11} and $\Delta\sigma_{11}$ of the reduced FFT-based microstructure simulation,

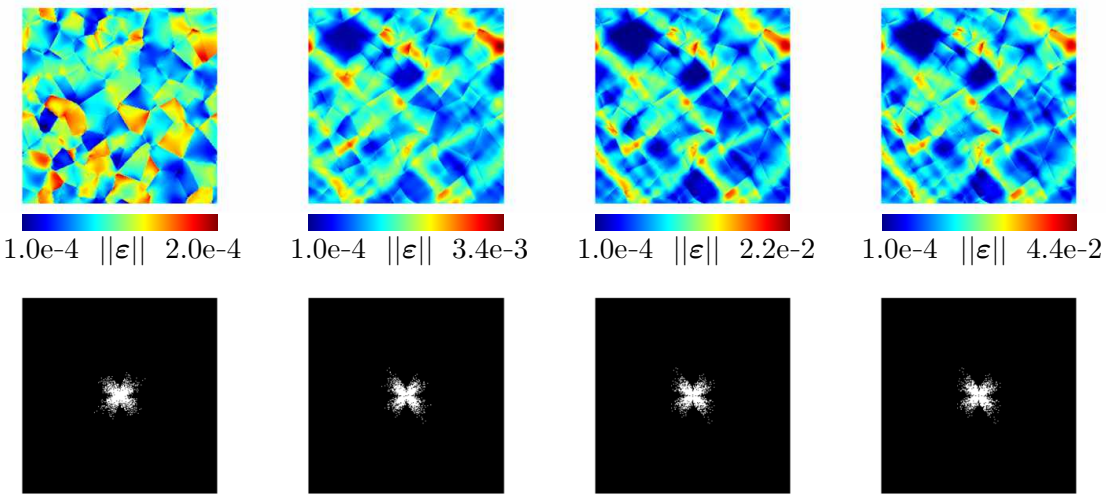

Figure 2: Norm of the strain field $||\boldsymbol{\varepsilon}||$ and corresponding strain-based sampling pattern with $\mathcal{R} \approx 0.8\,\%$ of considered Fourier modes for load steps 2, 20, 50 and 100 (from left to right).

considering $\mathcal{R} = 0.8\,\%$ and $\mathcal{R} = 11.6\,\%$ of Fourier modes and the reference solution are shown in Figure 3. It can be seen, that even by taking into account only $\mathcal{R} = 0.8\,\%$ of Fourier modes, the solution for the presented stress field σ_{11} is quite similar to the reference solution. This is confirmed by the differences within the microstructural stress field $\Delta\sigma_{11}$. As expected, by incorporating a larger amount of Fourier modes, such as $\mathcal{R} = 11.6\,\%$, these differences become even smaller.

Corresponding results can also be seen by looking at the overall macroscopic and microscopic

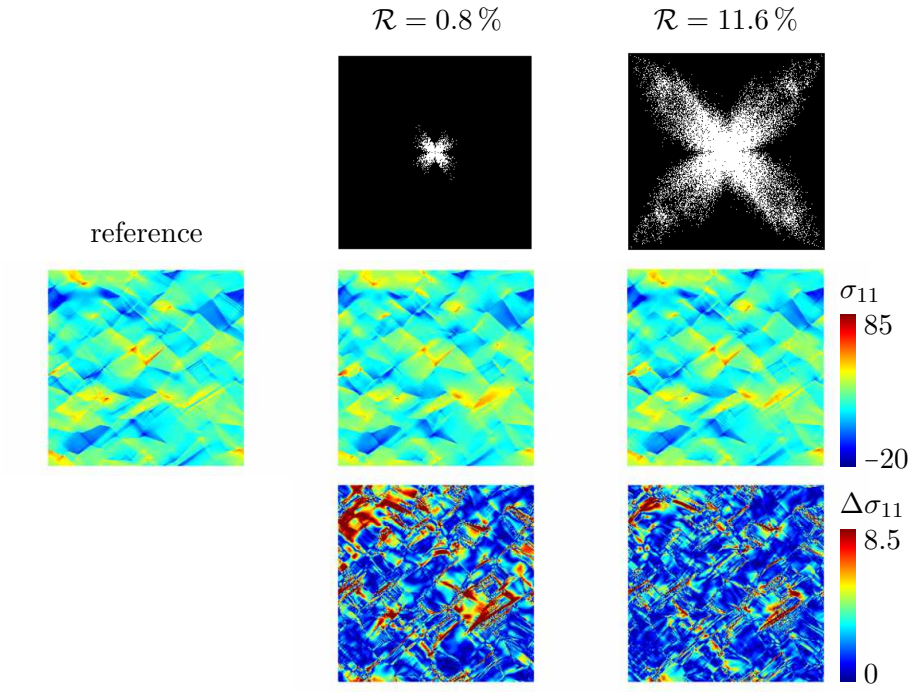

Figure 3: Microstructural fields: *Top row:* Strain-based sampling pattern for $\mathcal{R} = 0.8\,\%$ and $\mathcal{R} = 11.6\,\%$ of Fourier modes. *Middle row:* Corresponding and reference stress fields σ_{11}. *Bottom row:* Difference in the stress fields $\Delta\sigma_{11}$.

errors $\mathcal{E}$ and $\bar{\mathcal{E}}$, shown in Figure 4. Both error measures decrease with higher number of Fourier modes. In addition Figure 4 shows the relative CPU time t. Utilizing $\mathcal{R} = 0.8\,\%$ of Fourier modes the CPU times may for example be decreased by 60 %.

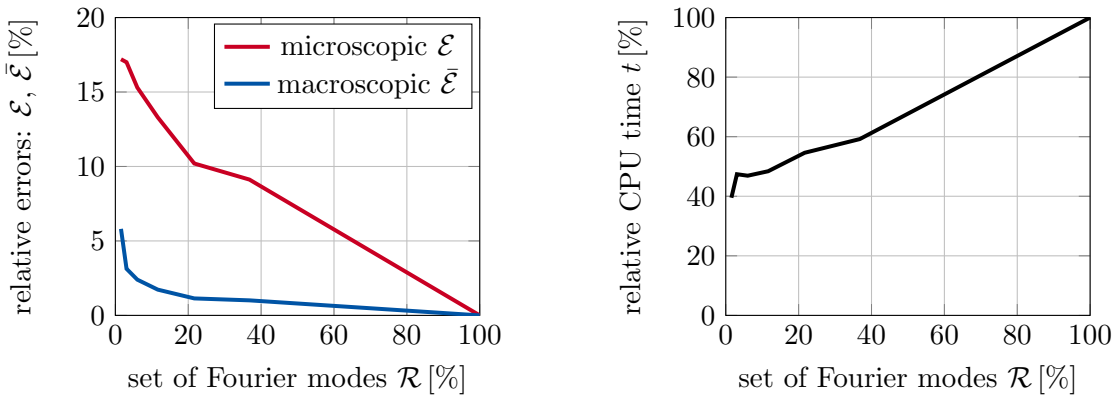

Figure 4: Macroscopic error $\bar{\mathcal{E}}$ (*left*) and microscopic error $\mathcal{E}$ (*right*) for the 2D elastic microstructure with one circular inclusion depending on the percentage of used Fourier modes $\mathcal{R}$ for the solution with the fixed and adapted sampling pattern.

5 CONCLUSION AND OUTLOOK

We presented the application of the reduced FFT-based microstructure simulation utilizing a reduced set of Fourier modes for the simulation of complex microstructures, such as polycrystals. To bypass the difficulties of defining a geometrically adapted sampling pattern for a polycrystalline microstructure, we used a strain-based sampling pattern for the choice of considered Fourier modes. Doing that, a reduction of CPU time of up to 60 % was achieved, while the microscopic and macroscopic errors are reasonably low.
Up to now, we used the MOR technique only in terms of the basic fixed point scheme, introduced by Moulinec and Suquet. Since much more efficient solvers are available nowadays, in future works we will consider the application of using a reduced set of Fourier modes with different solvers, such as fast gradient methods [1, 21] to reduce the computational costs in general. In addition, we will show the application of the MOR technique considering a strain-based sampling pattern, which evolves with increasing loading, to evolving microstructures by considering for example polycrystals incorporating phase transformations [26]. Furthermore, to reduce the effect of Gibbs oscillations [3] on the convergence behavior, we will also consider first- [27, 28] and higher-order [24] finite difference approximations of the differential operators within the spectral solver.

Acknowledgements: The authors gratefully acknowledge the financial support of the research work by the German Research Foundation (DFG, Deutsche Forschungsgemeinschaft) within the transregional Collaborative Research Center SFB/TRR 136, project number 223500200, subprojects M03 and M05. In addition Stefanie Reese gratefully acknowledges the financial support of the research work by the German Research Foundation (DFG, Deutsche Forschungsgemeinschaft) within the transregional Collaborative Research Center SFB/TRR 280, project number 417002380, subproject A01 and the project "Model order reduction in space and parameter dimension - towards damage-based modeling of polymorphic uncertainty in the context of robustness and reliability", project number 312911604, from the priority program (SPP) 1886.

REFERENCES

[1] Ernesti, F., Schneider, M. and Böhlke, T. Fast implicit solvers for phase-field fracture problems on heterogeneous microstructures *Comput Methods Appl Mech Eng* (2020) **363**:112793.

[2] Garcia-Cardona, C., Lebensohn, R.A. and Anghel, M. Parameter estimation in a thermoelastic composite problem via adjoint formulation and model reduction *Int. J. Numer. Methods Eng.* (2017) **112 (6)**:578–600.

[3] Gibbs, J.W. A Fourier's Series *Nature* (1898) **59**:200-200.

[4] Gierden, C., Kochmann, J., Waimann, J., Kinner-Becker, T., Sölter, J., Svendsen, B. and Reese, S. Efficient two-scale FE-FFT-based mechanical process simulation of elasto-viscoplastic polycrystals at finite strains *Comput Methods Appl Mech Eng* (2021) **374**:113566.

[5] Gierden, C., Waimann, J., Svendsen, B. and Reese, S. A geometrically adapted reduced set of frequencies for a FFT-based microstructure simulation *Comput Methods Appl Mech Eng* (2021) **386**:114131.

[6] Gierden, C., Waimann, J., Svendsen, B., and Reese, S. FFT-based simulation using a reduced set of frequencies adapted to the underlying microstructure *Comput. Methods Mater. Sci.* (2021) **21 (1)**:51–58.

[7] Gierden, C., Kochmann, J., Waimann, J., Svendsen, B. and Reese, S. A Review of FE-FFT-Based Two-Scale Methods for Computational Modeling of Microstructure Evolution and Macroscopic Material Behavior *Arch Computat Methods Eng* (2022), 1–21.

[8] Hashin, Z. and Shtrikman, S. On some variational principles in anisotropic and nonhomogeneous elasticity *J Mech Phys Solids* (1962) **10 (4)**:335–342.

[9] Kochmann, J., Wulfinghoff, S., Reese, S., Mianroodi, J.R. and Svendsen, B. Two-scale FE-FFT- and phase-field-based computational modeling of bulk microstructural evolution and macroscopic material behavior *Comput Methods Appl Mech Eng* (2016) **305**:89–110.

[10] Kochmann, J., Wulfinghoff, S., Ehle, L., Mayer, J., Svendsen, B. and Reese, S. Efficient and accurate two-scale FE-FFT-based prediction of the effective material behavior of elasto-viscoplastic polycrystals *Comput. Mech.* (2018) **61 (6)**:751–764.

[11] Kochmann, J., Manjunatha, K., Gierden, C., Wulfinghoff, S., Svendsen, B. and Reese, S. A simple and flexible model order reduction method for FFT-based homogenization problems using a sparse sampling technique *Comput Methods Appl Mech Eng* (2019) **347**:622–638.

[12] Köbler, J., Magino, N., Andrä, H., Welschinger, F., Müller, R. and Schneider, M. A computational multi-scale model for the stiffness degradation of short-fiber reinforced plastics subjected to fatigue loading *Comput Methods Appl Mech Eng* (2021) **373**:113522.

[13] Kröner, E. *Statistical Continuum Mechanics*. Springer-Verlag, Vol. 92, (1972).

[14] Lebensohn, R.A. N-site modeling of a 3D viscoplastic polycrystal using Fast Fourier Transform *Acta Mater.* (2001) **49 (14)**:2723–2737.

[15] Lebensohn, R.A., Kanjarla, A.K. and Eisenlohr, R. An elasto-viscoplastic formulation based on fast Fourier transforms for the prediction of micromechanical fields in polycrystalline materials *Int. J. Plast.* (2012) **32**:59–69.

[16] Lucarini, S., Upadhyay, M.V. and Segurado, J. FFT based approaches in micromechanics: fundamentals, methods and applications *Model. Simul. Mater. Sci. Eng.* (2021) **30**:023002.

[17] Moulinec, H. and Suquet, P. A fast numerical method for computing the linear and nonlinear mechanical properties of composites *C. R. Acad. Sci., Série II b* (1994) **318 (11)**:1417–1423.

[18] Moulinec, H. and Suquet, P. A numerical method for computing the overall response of nonlinear composites with complex microstructure *Comput Methods Appl Mech Eng* (1998) **157 (1–2)**:69–94.

[19] Perzyna, P. Thermodynamic theory of viscoplasticity *Adv. Appl. Mech.* (1971) **11**:313–354.

[20] Roters, F., Eisenlohr, P., Hantcherli, L., Tjahjanto, D.D., Bieler, T.R. and Raabe., D. Overview of constitutive laws, kinematics, homogenization and multiscale methods in crystal plasticity finite–element modeling: Theory, experiments, applications *Acta Mater.* (2010) **58 (4)**:1152–1211.

[21] Schneider, M. An FFT-based fast gradient method for elastic and inelastic unit cell homogenization problems *Comput Methods Appl Mech Eng* (2017) **315**:846-866.

[22] Schneider, M. A review of nonlinear FFT-based computational homogenization methods *Acta Mech.* (2021) **232**:2051–2100.

[23] Spahn, J., Andrä, H., Kabel, M. and Müller, R. A multiscale approach for modeling progressive damage of composite materials using fast Fourier transforms *Comput Methods Appl Mech Eng* (2014) **268**:871–883.

[24] Vidyasagar, A., Tan, W.L. and Kochmann, D.M. Predicting the effective response of bulk polycrystalline ferroelectric ceramics via improved spectral phase field methods *J. Mech. Phys. Solids* (2017) **106**:133–151.

[25] Vondřejc, J., Liu, D., Ladecký, M. and Matthies, H.G. FFT-based homogenisation accelerated by low-rank tensor approximations *Comput Methods Appl Mech Eng* (2020) **364**:112890.

[26] Waimann, J., Junker, P. and Hackl, K. Modeling the Cyclic Behavior of Shape Memory Alloys *Shape Mem. Superelasticity* (2017) **3 (2)**:124–138.

[27] Willot, F., Abdallah, B. and Pellegrini, Y.P. Fourier-based schemes with modified Green operator for computing the electrical response of heterogeneous media with accurate local fields *Int. J. Numer. Methods Eng.* (2014) **98 (7)**:518–533.

[28] Willot, F. Fourier-based schemes for computing the mechanical response of composites with accurate local fields *CR Mécanique* (2015) **343 (3)**:232–245.

[29] Wulfinghoff, S. and Böhlke, T. Equivalent plastic strain gradient crystal plasticity – Enhanced power law subroutine *GAMM-Mitt.* (2013) **36 (2)**:134–148.